Full Paper

Molecular Dynamics Simulations of the Growth of Thin a-C:H Films Under Additional Ion Bombardment: Influence of the Growth Species and the Ar⁺ Ion Kinetic Energy**

By *Erik Neyts,* *Maxie Eckert*, and *Annemie Bogaerts*

Molecular dynamics (MD) simulations are used to investigate the growth of thin, amorphous, hydrogenated carbon films for conditions corresponding to an argon/acetylene expanding thermal plasma with additional ion bombardment. It is shown that the hydrocarbon growth species determines the final structure of the film, in particular how the Ar⁺ ions contribute to the growth process. Attention is focused on how the Ar⁺ ion energy and flux influence the morphology of the films, the hydrogen content, the density, and the carbon coordination in the films due to a knock-on penetration mechanism.

Keywords: Film growth, Hydrogenated amorphous carbon, Ion bombardment, Molecular dynamics simulations

1. Introduction

Diamond-like carbon (DLC) thin films have been studied extensively since their first preparation in the early 1970s,[1] both by experimental and computational means. DLCs occur in a wide variety of compositions, ranging from real diamond-like materials to glassy carbon structures and hydrogenated polymeric films,[2] giving rise to their unique properties.

The diamond-like materials can be classified into two groups: hard 'tetrahedral amorphous carbon' (ta-C), and the softer a-C:H. The ta-C films generally have a high hardness and Young's modulus, a low roughness, and a very low friction coefficient.[2,3] When hydrogen is incorporated into this type of film, tetrahedral hydrogenated amorphous carbon, or ta-C:H, is obtained. These films are used, for example, as wear-resistant coatings on, e.g., magnetic hard disks and optical components. Experimentally, these materials are often fabricated using an ion-source, producing high-energy carbon or hydrocarbon ions (~100 eV) bombarding the substrate. The high-energy ions can penetrate into the sub-surface layers, or push surface atoms into the film, thereby causing a local increase in the density. These processes are called subplantation and knock-on penetration,

respectively. According to this new density, the local bonding will then reform, leading to a high sp³ fraction.[2]

The softer type of materials, which can be referred to as (hydrogenated) amorphous carbon, or a-C(:H), still exhibit a considerable hardness, with values of up to 20 GPa and even more, good adhesion, and chemical stability,[4,5] and can be used as, e.g., solid lubricants. These types of films can be produced by, e.g., plasma-enhanced (PE) CVD.[2] In contrast to the deposition of ta-C(:H), the ion flux fraction is now much lower than 100 %, the exact value depending on the type of source used. If high-energy ions are present, they can still contribute to the film growth by the same mechanism as for ta-C. However, in this case, neutral species will also contribute to the growth. The contribution of the neutral species will depend on their individual sticking coefficients. Diradicals can insert directly into surface C–C or C–H bonds, such that their sticking coefficient approaches 1. Monoradicals cannot insert directly into surface bonds, but need a dangling bond at the surface. This dangling bond can be created by removal of a hydrogen atom from a C–H surface bond, either by ion displacement of H, or by H-abstraction.[2,6] Closed-shell neutrals show sticking coefficients close to zero, and their effect is negligible. In contrast to the subplantation mechanism in ta-C(:H) growth, which is a physical process, the deposition mechanism of a-C(:H) films occurs through a combination of physical subplantation and chemical surface reactions if ions are present, or entirely through chemical reactions if no ions are present. Whether the subplantation mechanism and/or the knock-on penetration will be important under these conditions depends on the ion/radical flux ratio and the ion energy.

An efficient source to deposit a-C:H films is the so-called expanding thermal plasma (ETP).[7,8] In this type of source,

[*] Dr. E. Neyts, M. Eckert, Prof. A. Bogaerts
    Plasma, Laser Ablation and Surface Modeling ANTwerp
    (PLASMANT)
    Universiteitsplein 1, 2610 Antwerp (Belgium)
    E-mail: erik.neyts@ua.ac.be

no substrate bias has to be applied to obtain high-quality films,[9] with a hardness up to 14 GPa. Also, the deposition rate that can be achieved is very high, up to 70 nm s^{-1}, while preserving the quality of the films.[7,9] Most of the plasma chemistry and some of the particle/surface interactions have already been elucidated.[7,9] It was established that the major growth species depend on the ratio (F) between the C_2H_2 load, and the Ar$^+$ and electron fluence emanating from the arc. At low C_2H_2 fluxes ($F < 1$), mainly small species, such as C and C_2, contribute to the growth of the films. The obtained films are rather soft and show high roughness. At high C_2H_2 flows ($F > 1$), it was established using threshold ionization mass spectrometry (TIMS) that C_3 and C_3H are the major growth species.[10] Deposition then occurs at a high rate, up to 70 nm s^{-1}, and films with a considerable hardness (14 GPa), refractive index (2.2), and low roughness (3.7 nm) are obtained.[7,8]

In this study, we have investigated the growth of thin a-C:H films from hydrocarbon growth species characteristic for an ETP, when additionally a bias at the substrate is applied, so that Ar$^+$ ions from the plasma can be accelerated to the substrate. These ions will not be incorporated into the growing film, but they can give rise to knock-on penetration. Hence, we want to elucidate the role of the knock-on penetration mechanism on the structure of the films.

2. Description of the Model

The simulation model used in this work is based on the model developed by Tanaka et al.[11] In an MD model, all atoms in the system are followed through space and time by Newtonian mechanics. Particles move under the influence of forces, derived from an interatomic potential. In this work, the Brenner potential for hydrocarbons is used.[12] The C–F interaction parameters from the work of Tanaka et al. were replaced by the original interaction parameters for C–H interactions, taken from the work of Brenner.[12] This interatomic potential is a so-called bond-order potential, based on the Abell-Tersoff formalism,[13,14] where all the many-body chemistry is modeled by a bond-order function. In this approach, the total binding energy is written as a sum of nearest-neighbor pair interactions, modified by the local atomic environment, and thus allows for many-body interactions. To account for the specific hydrocarbon chemistry, such as the overbinding of radicals or conjugation effects, several correction functions were included. A description of the total C–C and C–H potential can be found in the original paper by Brenner.[12] The interaction potential for Ar-C and Ar-H is taken from Smith.[15]

The atom's spatial trajectory is integrated explicitly by using the velocity Verlet scheme.[16] The initial surface on which the growth of the a-C:H film is initiated was a previously simulated DLC film, containing 510 atoms, of which 4 % is hydrogen. The lower 128 atoms were kept static (corresponding to about 2 atomic layers), to anchor

the simulation cell, and to simulate a thick substrate. This initial substrate was produced by growing a film on a non-passivated, non-reconstructed diamond {111} surface, at a temperature of 523 K. The method and growth species used to produce this initial substrate are the same as for the deposition of the a-C:H films as explained below.

The deposition process was simulated by exposing the substrate continuously to hydrocarbon species and Ar$^+$ ions. In total, 15 films were deposited, corresponding to three series each of five films. The series differ from each other in the relative fluxes of the species bombarding the substrate, which are given in Table 1. The species and their fluxes are adopted from ETP experiments. In the ETP set-up, an Ar plasma is created in a cascaded arc, operated at sub-atmospheric pressure. The Ar plasma then expands

Table 1. Species and their relative fluxes as used in the simulations.

species	C	C_2	C_2H	l-C_3	c-C_3	l-C_3H	c-C_3H	C_5	C_5H	Ar$^+$
series I	0.299	0.157	0.031	0.024	0.024	0.0	0.0	0.0	0.0	0.465
series II	0.0	0.052	0.032	0.206	0.206	0.035	0.035	0.103	0.013	0.317
series III	0.0	0.0	0.0	0.287	0.287	0.053	0.053	0.156	0.062	0.102

into a low-pressure reaction vessel. The hydrocarbon gas is admixed into the emanating plasma by means of an injection ring placed at the top of the reaction vessel. The species and their fluxes correspond to absolute fluxes of the acetylene gas of 2.3 sccs ($F = 0.58$, Series I), 4.3 sccs ($F = 1.08$, Series II), and 17.7 sccs ($F = 4.4$, Series III), injected in the reactor chamber. More information regarding the ETP experiments can be found in the literature.[7,9,10]

As can be seen in Table 1, the small growth species, such as C and C_2, are mainly important in Series I; in Series II, the relative fluxes of these species are smaller, while bigger growth species such as the linear C_3 (l-C_3) and C_5, and the cyclic C_3 (c-C_3) become more important. In Series III, the relative flux of these species increases further compared to Series II. The relative flux of the Ar$^+$ ions is largest in Series I and smallest in Series III.

In order to investigate the effect of knock-on penetration on the structure of the resulting films, the kinetic energy of the Ar$^+$ ions was varied within each series, between 0.13 eV and 100 eV, as indicated in Table 2.

All impacts are normal to the surface, with a predefined kinetic energy of 0.13 eV per molecule for the neutral species, corresponding to an experimentally determined temperature of 1500 K. The incident particle was initially placed at a distance above the substrate beyond the cut-off of the potential. The position in the x and y directions was chosen randomly. Each trajectory is run for 20 000 time-

Table 2. Kinetic energy of the Ar$^+$ ions as used in the simulations.

Films	Ia, IIa, IIIa	Ib, IIb, IIIb	Ic, IIc, IIIc	Id, IId, IIId	Ie, IIe, IIIe
E_{Ar^+} [eV]	0.13	5.0	20.0	50.0	100.0

steps, equal to 2.0 ps per impact. Periodic boundary conditions were enforced in the $\pm x$ and $\pm y$ directions. The substrate temperature was cooled back to 523 K after 1.6 ps of each trajectory, using the Berendsen heat bath algorithm.[17] An invariable timestep of 0.1 fs was chosen. Currently, surface migration of atoms is not yet included in the model.

Reflected atoms, fragments, and molecules not bound to the surface are removed at the end of each trajectory. After deposition, the film is allowed to relax for 2.0 ps at a constant temperature of 523 K, after which the output data are obtained.

3. Results and Discussion

Results obtained with the simulations include the atomic H concentration in the films, the carbon coordination, the density of the films, and information about the structural properties. In addition to this structural information, the results also include information about the role of the different growth species and the mechanisms governing the deposition process.

3.1. General Structure of the Calculated Films

In Figure 1, representative parts of all 15 calculated structures are shown. It can be seen in the figure that films with different characteristics are obtained; the films from Series I have the highest density, while the films of Series III have the lowest density. This can be due to either the different growth species, the different Ar+ flux, or a combination of both. It will be shown below that at low Ar+ energies (Films Ia, IIa, and IIIa), the increase in density is entirely due to the different nature of the growth species. At high Ar+ energy (Films Ie, IIe, and IIIe), this effect remains operative, but the Ar+ flux will then act as an additional factor also contributing to the density increase.

Second, it can be seen from the figure that increasing the kinetic energy of the Ar+ ions also increases the density of the films. The density of Film Ie (Ar+ energy of 100 eV) is clearly higher as compared to the density of Film Ia (Ar+ energy of 0.13 eV).

It should be noted that in the experiments the highest densities were obtained for an acetylene flux of 17.7 sccs, i.e., corresponding to simulation Series III, while the lowest densities were obtained for an acetylene flux of 2.3 sccs, corresponding to simulation Series I.[5] However, it is probable that there is an additional H flux towards the substrate in the experiment that could not be measured,[5] and which is therefore not included in the present simulations. Also, MD simulations are limited to short time scales, such that long time effects (e.g., relaxation) that might be important are not included. Nevertheless, all obtained simulation results can be explained consistently (see below). Finally, the present paper focuses on the effect of Ar+ ion bombardment due to a bias at the substrate, which was not yet applied in the experiments cited.[5]

From Figure 1, it is also clear that the growth species, Ar+ ion flux, and energy also determine the average carbon coordination numbers. Again, both the growth species and the relative Ar+ flux influence the coordination numbers comparing Series I, II, and III, as will be explained below. Within each series, the carbon coordination number will increase as the Ar+ energy increases. This can be seen in the films from Series II, clearly showing an increase in the fraction of 3-coordinated carbon atoms as the Ar+ energy increases. Finally, it will also be shown how these factors influence the H content in the films, and how these results are consistently connected to each other.

Film Ia	Film Ib	Film Ic	Film Id	Film Ie
Film IIa	Film IIb	Film IIc	Film IId	Film IIe
Film IIIa	Film IIIb	Film IIIc	Film IIId	Film IIIe
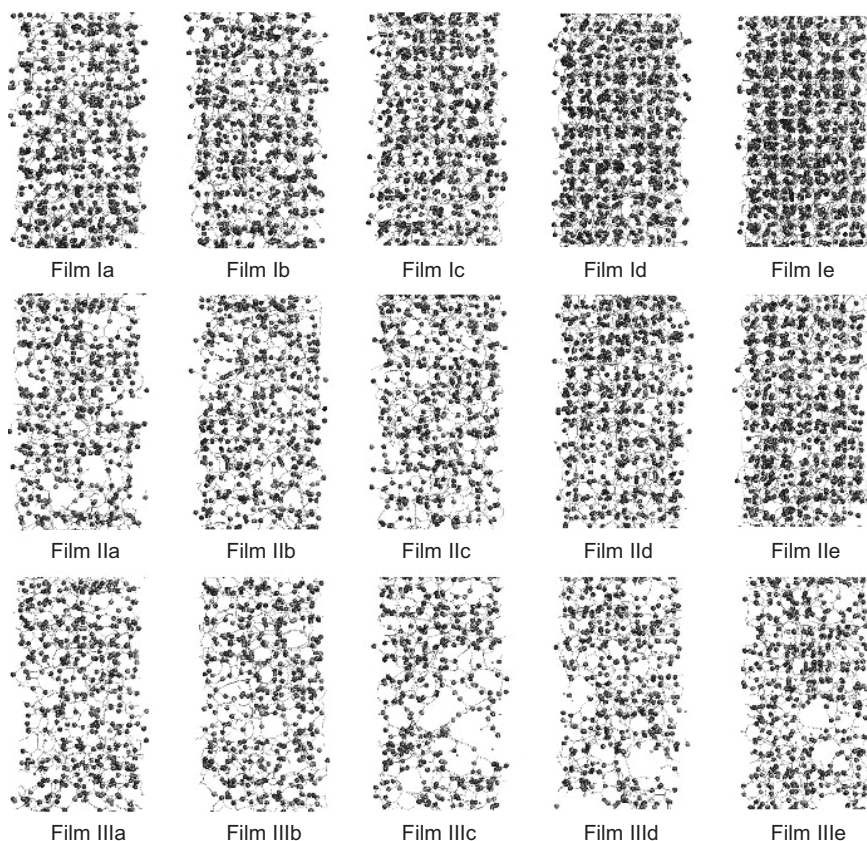
Fig. 1. Representative parts of the structure of all calculated films as seen from the side.

Hence, it is clear that the growth species, the relative flux of the Ar^{+} ions, and the Ar^{+} ion energy are of great importance in determining the film structure. In the following sections, the characteristics of the different films will be discussed in more detail.

3.2. Density of the Films

In Figure 2, the densities of the different films are shown as a function of the Ar^{+} ion energy for the three series. From the figure it is clear that the density of the deposited films is dependent on the simulated conditions, i.e., the Ar^{+}
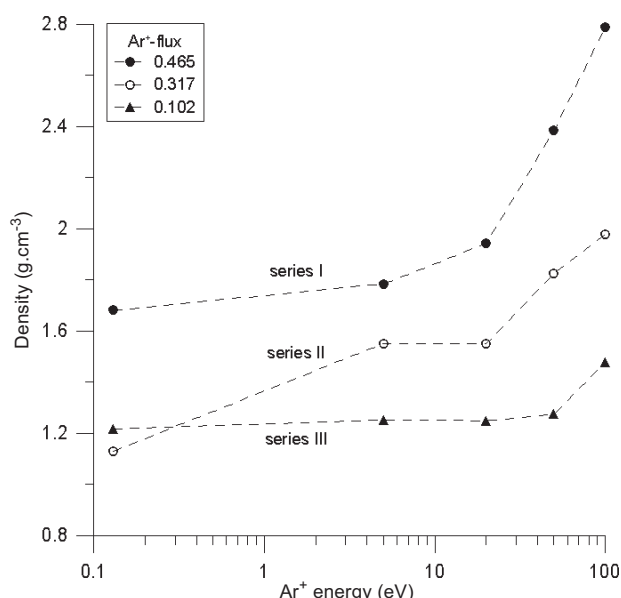
Fig. 2. Calculated mass densities of the films as a function of the Ar^{+} ion energy.

ion energy and flux, and the nature of the growth species. At the lowest Ar^{+} ion energy, the influence of the Ar^{+} ions is negligible.[2] Therefore, at these energies, the differences in density between the various series can be attributed to the different nature of the growth species. We shall therefore discuss the influence of the growth species first.

The films from Series I have the highest density, as can been seen in Figure 2. Recall that in this series, the main growth species are the small C and C_2 radicals. The relative fluxes of these species are smaller in Series II, where the main growth species are C_3 and C_3H. This transition reflects the importance of the C and C_2 species as contributing factors to the high density of the films in Series I (see below). In Series III, there are no C and C_2 species present, and the main growth species are now the C_3 and C_3H species, as well as a considerable fraction of C_5 particles. These films have the lowest densities.

When the larger (linear) species l-C_3, l-C_3H, C_5, and C_5H stick on the surface of the growing film, these molecules

screen part of the surface for new incoming particles. It is clear that this will finally lead to a low overall density in the film. Also, these species have strong interatomic bonds, such that they do not break up upon impact, in contrast to the cyclic species.[18] The small species, however, are small enough to ensure a more homogeneous coverage of the surface, leading to a higher density. Furthermore, the larger species generally only bind to the surface with only one bond, while the smaller species tend to bind to multiple atoms on the surface. Hence, it can be concluded that large relative fluxes of the larger growth species will induce a lower density of the resulting film.

Although the simulation results can be explained self-consistently as shown above, it also follows from these results that the input conditions in the simulations do not correspond exactly to the experiments under the high acetylene flux conditions. Indeed, while an increase in density is seen with increasing acetylene flow in the experiment, a decrease is seen in the simulations. This is probably due to the fact that: a) only those species of which it is known that they are growth species under the given conditions are included in the simulations, while it is probable that other (yet unidentified) growth species are present as well under high acetylene flow conditions; b) the ratio between linear and cyclic growth species could not be measured experimentally, while we have already shown in the past that this ratio influences the resulting film properties;[18] and c) the fluxes of the different growth species are subject to uncertainties, and it is not known to what extent these uncertainties influence the resulting film properties.

As already mentioned above, the Ar^{+} ions also strongly influence the density of the films. Generally, the density increases both with ion energy and ion flux. This observation can be explained by the mechanism of knock-on penetration, where Ar^{+} ions can push surface atoms in the growing film, thereby causing a local increase in density. The absolute number of knock-on penetration events will increase as the relative frequency of impinging Ar^{+} ions (i.e., the relative Ar^{+} flux) increases. This will then lead to a higher density of the film. On the other hand, increasing the ion energy will increase the probability of inducing a knock-on event per impinging Ar^{+} ion. Therefore, also increasing the ion energy will increase the density of the films. This can be clearly seen in Figure 2, at high ion energies.

Both effects are cumulative, i.e., increasing the Ar^{+} ion energy when a high ion flux is present will increase the density more strongly, while increasing the ion energy when a low ion flux is present will only slightly increase the density. For example, compare the increase in density when the ion energy is increased from 50 eV to 100 eV; when the relative Ar^{+} flux is low (0.102), the density increase is only 0.2 g cm^{-3}, while the density increase is about double (0.4 g cm^{-3}) when a high relative Ar^{+} flux of 0.465 is present.

To summarize, at the lowest Ar^{+} ion energies, the Ar^{+} ions have little influence, since they are not able to induce

knock-on penetration events. Therefore, only the nature of the growth species determines the differences in density between the different series at these low ion energies. As the ion energy increases, this effect of the growth species remains operative. However, the Ar^+ ion flux and energy then also become additional factors intensifying the differences in film densities, as explained above. This explains why the differences in densities of the films are larger at high ion energies than at low ion energies.

3.3. Coordination in the Films

The calculated average carbon coordination numbers (Z_C) in the bulk of the films are given in Figure 3, where it is clear that this number is dependent on the chosen deposition conditions. Again, a distinction can be made be-
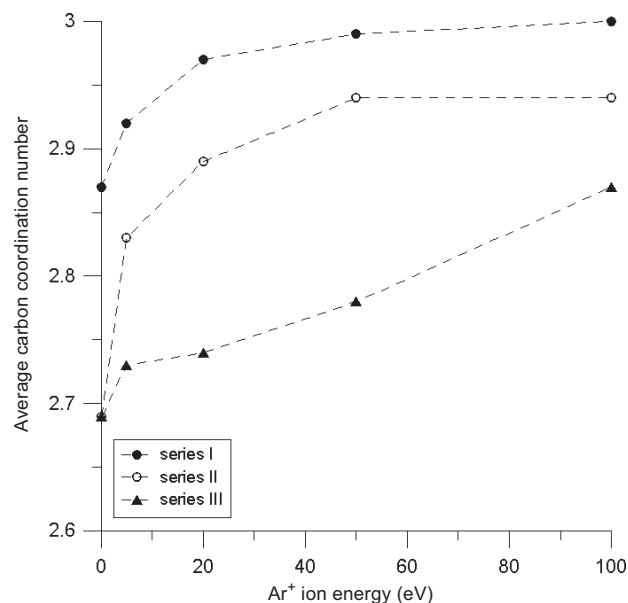
Fig. 3. Calculated average carbon coordination number in the various films as a function of the Ar^+ energy.

tween the influence of the growth species on the one hand, and the influence of the Ar^+ ions on the other hand. At low Ar^+ ion energy, the influence of the growth species will be dominant, since the ion energy is too low to induce knock-on penetration events. The relative effect of the Ar^+ ions increases as their kinetic energy increases, as was explained earlier (see above).

The films from Series I have the highest average carbon coordination number (i.e., between 2.9 and 3), while the growth species are mainly small – about 85 % of the impinging growth particles are C and C_2 radicals. In Series II and III, the main growth species are l-C_3 and c-C_3, accounting for about 60 % of all impacts. In Series III, the growth species are bigger as compared to Series II (more C_5, C_3H, and no C_2 or C_2H). These data therefore indicate that the

nature of the growth species, both in size and structure, influences the average coordination; the larger the fluxes of the large growth species, the lower the resulting average carbon coordination.

Indeed, when a C-atom sticks to the surface, it will form at least one bond, leaving three valence electrons on the C-atom available for the formation of subsequent bonds. Therefore, the impingement of one C-atom on the surface allows the formation of at least one more bond and at most three other bonds, corresponding to a coordination number of at least two and at most four. The larger species, however, have only one valence electron to bind to the surface, since they are monoradicals. Most carbon atoms of such a larger particle will therefore be 2-coordinated after sticking to the surface. Also, the atoms in these larger impacting molecules are connected to each other by strong multiple bonds. Therefore, a new incoming particle cannot simply chemisorb onto one of these carbon atoms in order to increase the coordination number of this carbon atom. Hence, the average carbon coordination number will be higher when a large flux of small C-atoms is present (Series I), compared to when a large flux of the larger monoradicals is present (Series II and III).

Previously, we have reported a reasonable agreement between the calculated four-fold carbon coordination and the carbon sp^3 content as measured by EELS for conditions resembling the current low acetylene flow conditions.[19] However, we do not find such a correspondence under high acetylene fluxes, which further strengthens our belief that the conditions in the simulation and the experiment do not exactly correspond under these high acetylene flow conditions.

Furthermore, the average carbon coordination is also influenced by the Ar^+ ions. It can be seen in Figure 3 that the average carbon coordination increases with increasing Ar^+ ion energy in all three series. Recall that when a high energy ion impinges on the surface, knock-on penetration can occur; the Ar^+ ion collides on one of the surface atoms and pushes this atom into the growing layer. This causes a local increase of the density around the atom. It is then proposed that the atomic hybridization can easily change from sp to sp^2 to sp^3 due to this increased density.[2] Therefore, the average carbon coordination will increase with increasing Ar^+ energy and Ar^+ flux, identifying 1- and 2-coordinated carbon atoms with sp hybridization, as well as 3-coordinated carbon atoms with sp^2 hybridization and 4-coordinated carbon atoms with sp^3 hybridization.

3.4. Hydrogen Content in the Films

Finally, we have also investigated the effect of the growth species and the Ar^+ ions on the hydrogen fraction in the films. All hydrogen atoms in the simulated films originate from the impinging hydrocarbon growth species. Since the carbon atoms in the growth species are bound to a maxi-

mum of one hydrogen atom, and nearly all hydrogen atoms in the films are present in the form of CH fragments, it can be concluded that breaking of C–H bonds and subsequent migration of H atoms in the films is negligible.

The calculated average mole fractions of hydrogen in the bulk of the films in the different simulation series and the hydrogen mole fraction in the growth species are shown in Figure 4. From this figure, it is clear that the fractions of hydrogen in all films is lower than would be expected from the relative fluxes of the hydrocarbon growth species. Since migration of hydrogen in the growing films is unlikely, the smaller hydrogen mole fractions in the films (compared to the hydrogen mole fractions in the growth species) indicate mechanisms operative at the surface of the growing films.

One possible mechanism could be the sputtering of hydrogen atoms at the surface by impinging Ar^+ ions. If this would indeed be the main mechanism for removal of hydrogen from the surface, then the difference between the H fraction in the film and in the growth species should increase with increasing energy within each series. There is, however, no clear trend visible in going from film a to film e. Hence, sputtering of H atoms by impinging Ar^+ ions is not the main mechanism for removal of H from the films. Since the Ar^+ ions are not responsible for H removal, then the Ar^+ flux cannot be a contributing factor. Therefore, the differences in the H-content between the films from Series I, II, and III, in comparison with the mole fraction of H in the growth species, should be attributed to the different species contributing to growth of the films and to their different ability to abstract H from the surface of the growing film.

Indeed, in the past we have already demonstrated that the C_2 radical has a much higher ability to abstract H from the surface compared to C_3 and C_3H species.[20] This corresponds to the observation in the present simulations that removal of H from the films occurs to a much larger extent in Series I, where small species such as C and C_2 are the main growth species, compared to Series II and III, where the main growth species are the larger C_3 and C_3H species.
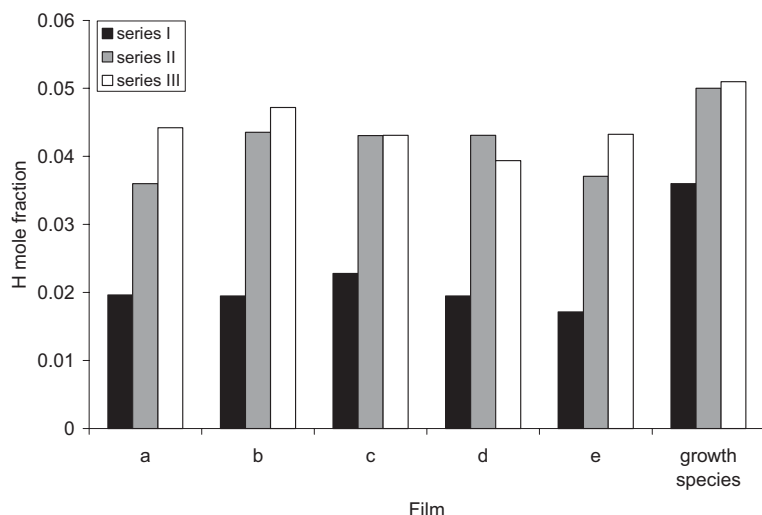
Finally, the precision of our simulations is difficult to estimate. Since the calculations are very time consuming, it is not feasible to repeat them a few times every run. However, previous simulations indicate that reproducibility of the results is expected to be in the order of 1–2 %.[21]

4. Conclusion

Classic molecular dynamics simulations were carried out to investigate the growth of thin amorphous hydrogenated carbon films (a-C:H) under conditions relevant for an acetylene/argon expanding thermal plasma. More specifically, the effect of the energy of Ar^+ ions and their relative flux, as well as the effect of the growth species and their fluxes on the structure of the resulting films was investigated. In total, 15 films were deposited, for acetylene loads of 2.3 sccs, 4.3 sccs, and 17.7 sccs, with film densities ranging from 1.1 $g\,cm^{-3}$ to 2.8 $g\,cm^{-3}$.

It is shown that the density of the films is dependent on the growth species, the Ar^+ relative flux, and energy. At low Ar^+ energies, the differences in densities between the films from the three series are due to the different nature of the growth species. Films grown from small growth species are generally denser compared to films grown from larger species. As the Ar^+ ion energy increases, the probability per Ar^+ ion impact for pushing a surface atom into the growing film (a knock-on penetration event) increases. The total number of knock-on penetration events is further determined by the Ar^+ flux. These knock-on penetration events cause an increase in the density of the film. Hence, the most dense films are obtained at high ion energy and high Ar^+ ion flux, grown from small growth species, while for large species, low ion energy and low ion flux lead to lower density films.

Also the calculated average carbon coordination number is strongly dependent on the nature of the growth species and on the Ar^+ ion bombardment. Indeed, it is shown that films grown from the small growth species invariably show higher average carbon coordination numbers compared to the films grown from larger species. Increasing the ion energy increases the carbon coordination, again by the mechanism of knock-on penetration.

Finally, the hydrogen fraction in the films was also investigated. In all films, the H mole fraction in the films is lower than would be calculated from the growth species. It is demonstrated that this is not due to sputtering of H atoms by energetic Ar^+ ions, but rather due to the ability of the growth species to abstract hydrogen from the surface. The smaller growth species espe-

Fig. 4. Calculated mole fractions of hydrogen in the various films and in the hydrocarbon growth species.

cially show this behavior, such that the films deposited from these species show the strongest decrease in H mole fraction relative to the H mole fraction present in the growth species.

[1] S. Aisenberg, R. Chabot, *J. Appl. Phys.* **1971**, *42*, 2953.
[2] J. Robertson, *Mater. Sci. Eng.* **2002**, *R37*, 129.
[3] J. Robertson, *J. Non-Cryst. Solids* **2002**, *299–302*, 798.
[4] http://www.bekaert.com/bac/Products/Diamond-Like%20Coatings.htm (accessed May 2007).
[5] J. Benedikt, *Ph.D. Thesis*, TU-Eindhoven, **2004**.
[6] A. von Keudell, T. Schwarz-Selinger, W. Jacob, *J. Appl. Phys.* **2001**, *89*, 2979.
[7] J. Benedikt, M. Wisse, R. V. Woen, R. Engeln, M. C. M. van de Sanden, *J. Appl. Phys.* **2003**, *94*, 6932.
[8] J. W. A. M. Gielen, M. C. M. van de Sanden, P. R. M. Kleuskens, D. C. Schram, *Plasma Sources Sci. Technol.* **1996**, *5*, 492.
[9] J. Benedikt, D. J. Eijkman, W. Vandamme, S. Agarwal, M. C. M. van de Sanden, *Chem. Phys. Lett.* **2005**, *402*, 37.
[10] J. Benedikt, S. Agarwal, D. Eijkman, W. Vandamme, M. Creatore, M. C. M. van de Sanden, *J. Vac. Sci. Technol. A* **2005**, *23*, 1400.
[11] J. Tanaka, C. Abrams, D. Graves, *J. Vac. Sci. Technol. A* **2000**, *18*, 938.
[12] D. W. Brenner, *Phys. Rev. B* **1990**, *42*, 9458.
[13] G. C. Abell, *Phys. Rev. B* **1985**, *31*, 6184.
[14] J. Tersoff, *Phys. Rev. Lett.* **1988**, *61*, 2879.
[15] R. Smith, *Atomic and Ion Collisions in Solids and at Surfaces*, Cambridge University Press, New York **1997**.
[16] W. C. Swope, H. C. Anderson, P. H. Berens, K. R. Wilson, *J. Chem. Phys.* **1982**, *76*, 637.
[17] H. J. C. Berendsen, J. P. M. Postma, W. F. van Gunsteren, A. DiNola, J. R. Haak, *J. Chem. Phys.* **1984**, *81*, 3684.
[18] E. Neyts, A. Bogaerts, M. C. M. van de Sanden, *J. Appl. Phys.* **2006**, *99*, 014902.
[19] E. Neyts, A. Bogaerts, R. Gijbels, J. Benedikt, M. C. M. van de Sanden, *Diamond Relat. Mater.* **2004**, *13*, 1873.
[20] E. Neyts, M. Tacq, A. Bogaerts, *Diamond Relat. Mater.* **2006**, *15*, 1663.
[21] E. Neyts, A. Bogaerts, M. C. M. van de Sanden, *Appl. Phys. Lett.* **2006**, *88*, 141922.